**International Journal of Power Electronics and Drive System (IJPEDS)**
Vol. 17, No. 3, September 2026, pp. 2210~2223
ISSN: 2088-8694, DOI: 10.11591/ijpeds.v17.i3.pp2210-2223 

# Adaptive predictive control for wind energy efficiency in real-time in smart grids

**Kadhim Hamzah Chalok[1], Karrar Hameed Kadhim[2]**
[1]Center for Research on Environment and Renewable Energy, University of Kerbala, Karbala, Iraq
[2]Al-Musaib Technical College, Al–Furat Al–Awsat Technical University, Kufa, Iraq

**Article Info**

***Article history:***

Received Feb 27, 2026
Revised Aug 18, 2026
Accepted Aug 24, 2026

***Keywords:***

Adaptive predictive control
Real-time optimization
Renewable integration
Smart grid
Turbine dynamics
Wind energy

**ABSTRACT**

With the increasing global interest in renewable energy, advanced control strategies for wind energy conversion systems (WECSs) are critical for achieving not only maximum efficiency but also grid compatibility. This paper introduces a new adaptive, forecast-based predictive control algorithm to maximize the real-time energy efficiency of wind turbines integrated with smart grid architectures. The method couples a short-term wind-speed prediction module with a model-predictive control algorithm that uses the predictions to anticipate and adjust turbine operating conditions, such as pitch angle and rotor speed, to counteract the mechanical load from wind shear while maximizing power production. The analysis employs a dataset of 487 high-resolution cases of wind speed and wind turbine performance metrics to train and validate the adaptive model. The simulations were conducted in MATLAB/Simulink, using a model that captures the turbine's nonlinear behavior and the electrical grid connection. The results indicate that the proposed controller increases the cycle-averaged power coefficient by approximately 8.2% and reduces tip-speed-ratio tracking error by roughly 70% relative to a conventional proportional–integral–derivative (PID) controller, while also reducing pitch and torque actuation, thereby lowering structural fatigue loads. This study is expected to provide a reliable solution to wind energy intermittency and facilitate the more stable and efficient integration of wind farms into modern smart grid systems.



***Corresponding Author:***

Kadhim Hamzah Chalok
Center for Research on Environment and Renewable Energy, University of Kerbala
56001 Karbala, Iraq
Email: kadhim.hamzah@uokerbala.edu.iq

## 1. INTRODUCTION

One major challenge of the 21st century is integrating renewable energy sources into the current grid system, as demonstrated by reviews of the evolution of wind-farm control technology [1]. With increasing demand for cleaner energy sources to mitigate environmental impacts and the depletion of fossil fuel resources, wind energy conversion systems, spanning onshore, offshore, and floating installations, have assumed a leading role in global energy generation, as documented in large-scale renewable deployment studies [2], [3]. However, the grid's reliability, stability, and efficiency have been greatly influenced by the stochastic nature of wind profiles [4]. Conventional control approaches may fail to adapt to sharp changes in wind speed. This leads to reducing the system's efficiency in power extraction and more expected failure of mechanical turbine components [5]. To address the aforementioned issues, new, more proactive and predictive control approaches are required. These methods can easily handle changes in environmental conditions and intelligently tune system parameters to improve performance. This is motivated by the developments and advances in control research [6]. The smart grid principle supports this by providing bidirectional communication and advanced data analytics, enabling real-time optimization of decentralized energy resources [7].

The grid is in an era in which the centralized, unidirectional nature of its conventional operation is giving way to a complex, decentralized network known as the smart grid [8]. This development necessitates the efficient integration of wind energy conversion (WEC) systems into the broader grid infrastructure [9]. Compared with dispatchable power plants, whose fuel inputs can be adjusted with high precision to match demand, wind farms are subject to unpredictable weather conditions [10]. This intermittency causes voltage and frequency fluctuations that could potentially contribute to grid instability if not properly regulated [4]. The grid also imposes stringent regulations for fault ride-through and reactive power support [11]. For integration strategies, advanced control interfaces are used to decouple the mechanical variation in the wind turbine from the electrical, consistent network requirements. The decoupling principle is introduced in the power electronics control source [12]. Wind systems are considered part of grid regulation, implying a paradigm shift, and have already been shown to provide active grid support in previous studies. The most difficult aspect is designing a control approach that achieves good peak-power tracking while also providing ancillary services, such as frequency regulation [13]. This means that the control structure must be grid-aware. It must not only modulate generation in the presence of wind but also react to the real-time requirements of the smart grid [14], [15]. Reliability is another important factor: drivetrain and bearing faults are among the major issues of wind turbine downtime. Therefore, developing a control approach that deals with both improving power tracking and mitigating mechanical stress [16].

The development of control systems for wind energy generation extends beyond conventional mechanical improvements to encompass more sophisticated, computer-based control approaches. Earlier methods focused mainly on constant-speed turbines, with control limited to passive pitch regulation or stall control [17]. A major drawback of these approaches is their reliance on linear controllers, which cannot adequately handle the nonlinear and rapidly changing aerodynamics of a wind turbine, particularly within the transition range between partial-load and full-load operation. As a result, research efforts have shifted toward more sophisticated nonlinear control techniques, such as fuzzy logic, neural networks, and robust control methodologies [18]. Data-driven, spatio-temporal forecasting frameworks have likewise been proposed to improve the accuracy of short-term wind power prediction [19], alongside Kalman-filter-based hybrid approaches for short-term wind speed prediction [20]. The inclusion of such prediction modules within the control loop itself is a relatively recent advance in this area, combining statistical forecasting with supervised control design. The merging of these two ideas – forecasting and control – led to the development of predictive control for wind turbines as a theoretical framework [2]. The theoretical benefits of integrating these have been discussed extensively in the academic literature, with load reduction and increased energy yield as the primary outcomes. Very recent work continues to push this direction: Bayesian self-optimization has been used to tune robust MPC weighting parameters online for utility-scale turbines [21], while multi-algorithmic adaptive machine-learning frameworks have been proposed to combine several forecasting models for short- and long-term wind energy prediction [22].

Most current research relies on offline or stationary predictive models, which may not capture the time-variant characteristics of turbine parameters arising from wear or changing environmental conditions [23]. Moreover, existing adaptive schemes rarely couple online forecast adaptation directly to a constrained, multi-objective optimal control law that, in real time, jointly balances power capture, structural fatigue, and grid-quality requirements, thereby limiting their practical robustness under highly variable wind conditions. The closest related work couples recursive-least-squares online identification with adaptive model predictive control (MPC) for load-frequency regulation under renewable disturbances, but is formulated at the grid-frequency level rather than at the turbine level, addressing fatigue and grid-quality objectives simultaneously [24]. This progression – from adaptive forecasting to today's most advanced predictive architectures [9], [25] – sets the stage for the forward-looking, adaptive framework proposed in this study.

This study presents an adaptive forecast-driven predictive control (AFDPC) framework that couples online recursive least squares wind-speed forecasting directly with a constrained, multi-objective model-predictive controller for turbine-level operation. Unlike the closest related work, which applies RLS-adaptive MPC at the grid-frequency level, or fixed-model MPC formulations that treat power capture, structural fatigue, and grid-quality as separate or offline-tuned objectives, AFDPC re-estimates its forecasting model online at every sampling instant and feeds the updated near-future wind-state prediction directly into a single cost function that jointly penalizes power-tracking error, drivetrain torque, and control effort. This tight coupling – an online-adaptive forecast feeding a multi-objective, turbine-level MPC within one closed loop – is what distinguishes AFDPC from the adaptive-forecasting and fixed-model MPC approaches reviewed above, and it is what allows the controller to exploit the rotor's aerodynamic performance to the fullest extent permitted by the electrical grid's operational constraints.

The significance of this work lies not only in increasing overall power production, but also in ensuring smoother power injections into the grid and thereby improving system-wide stability, an aim underlined by grid support strategy research. The presented framework is expected to benefit wind-farm operators by reducing mechanical wear and maintenance costs, and grid operators by providing more predictable and stable power injection. In this respect, the presented technique is expected to benefit wind farm operators by reducing mechanical wear, lowering maintenance costs, and providing more stable, predictable power injection. In doing so, the proposed approach achieves a favorable trade-off between maximizing mechanical energy harvesting and preserving power quality, consistent with the broader trade-offs inherent in multi-objective energy management. The remainder of this study examines the relationship among wind variability, grid requirements, and control architectures, addressing the main challenges posed by volatile renewable resources and fluctuating grid demand.

## 2. METHOD

### 2.1. Research design and approach

Model predictive control (MPC) is a flexible and widely used control method developed for the chemical process industry and subsequently extended to the automotive sector. This evolution from linear predictive control, which operates on linearized, simplified wind turbine models, to nonlinear predictive control, which uses the full aerodynamic equations, is discussed in an advanced modeling study. The primary benefit cited in most studies is the ability to address constraints systematically through constraint-optimization investigations [26], [27]. For example, a wind turbine has known physical limits on how quickly the blades can pitch and on the torque the generator can extract [18]. Recent developments in the literature address distributed predictive control of an entire wind farm, considering wake effects between upwind and downwind turbines for cooperative control [28]. The review identifies the frontiers of research in adaptive predictive control, in which the controller's internal model is unknown and is estimated in real time, thereby maintaining optimal performance even as a turbine's physical characteristics vary over time.

The control scheme proposed in this work is based on a hierarchical structure consisting of an estimation device and a nonlinear model-predictive controller. System implementation begins with the data collection layer, which acquires wind speed (WS), rotor speed (RS), blade pitch angle (BPA), and generator torque at regular intervals. This raw data is then passed to the adaptive prediction module. The proposed model is based on time-series forecasting of the effective wind-speed profile over a defined future time horizon. What makes this block novel is that the prediction is adaptive, as these parameters are recalculated online using a recursive algorithm that minimizes forecast error from previous time slots. It also keeps the forecast up to date whenever the weather contradicts expectations.

Once the future wind profile has been predicted, it is treated as an exogenous input to the predictive-control optimization problem, which is formulated around a mathematical model of the wind turbine's dynamics encompassing its aerodynamic, mechanical, and electrical subsystems. The optimization problem seeks to minimize a composite cost function that balances three competing objectives: maximizing power capture, minimizing structural fatigue (quantified via drivetrain shaft torque), and minimizing control effort (i.e., the rates of change of pitch angle and generator torque). The solver adopts a receding-horizon formulation, in which the optimal control-input trajectory is computed over the prediction horizon, but only its first element is extracted and applied to the actuators. At the next step, the prediction horizon is shifted forward, the system state is updated, the forecast is refreshed, and the optimization problem is solved again. Because this procedure operates in a closed loop, it can compensate for system errors and unmodeled disturbances. MATLAB/Simulink was used as the simulation environment. The turbine dynamics were represented using a high-frequency two-mass drivetrain model together with a realistic aerodynamic lookup table, enabling simulation of a multi-MW wind turbine connected to a stiff grid.

Figure 1 presents the simulation setup in MATLAB/Simulink for the AFDPC pipeline. It comprises five interrelated blocks: input and data, forecasting, control, actuation and plant, and grid and evaluation. In the first block, wind data is retrieved from a predefined wind profile and is then processed, filtered, and scaled in real time to serve as input. The data is subsequently passed to the Forecasting block, where an ARIMA model and a forecast core are used to produce short-term wind-speed forecasts over a 50-step horizon; these forecasts are updated online using a recursive least-squares algorithm, with the resulting error used to refine the model. The estimated wind and system state are then passed to the model predictive control stage, where a solver computes the optimal pitch and torque commands. These commands drive the aerodynamic rotor, drivetrain, and doubly fed induction generator (DFIG), governing the turbine's mechanical and electrical response to changing wind conditions. Throughout this process, two feedback loops maintain closed-loop stability: sensor data is returned to the state estimator as state feedback, while a separate connection between the forecast core and the prediction horizon provides adaptation feedback that refines the forecasting model. The resulting power then flows through the grid components, after which frequency and voltage checks assess grid quality before the performance log records the results. Together, this closed-loop design integrates predictive optimization, forecasting, grid-quality observation, and physical turbine dynamics into a reproducible simulation environment.

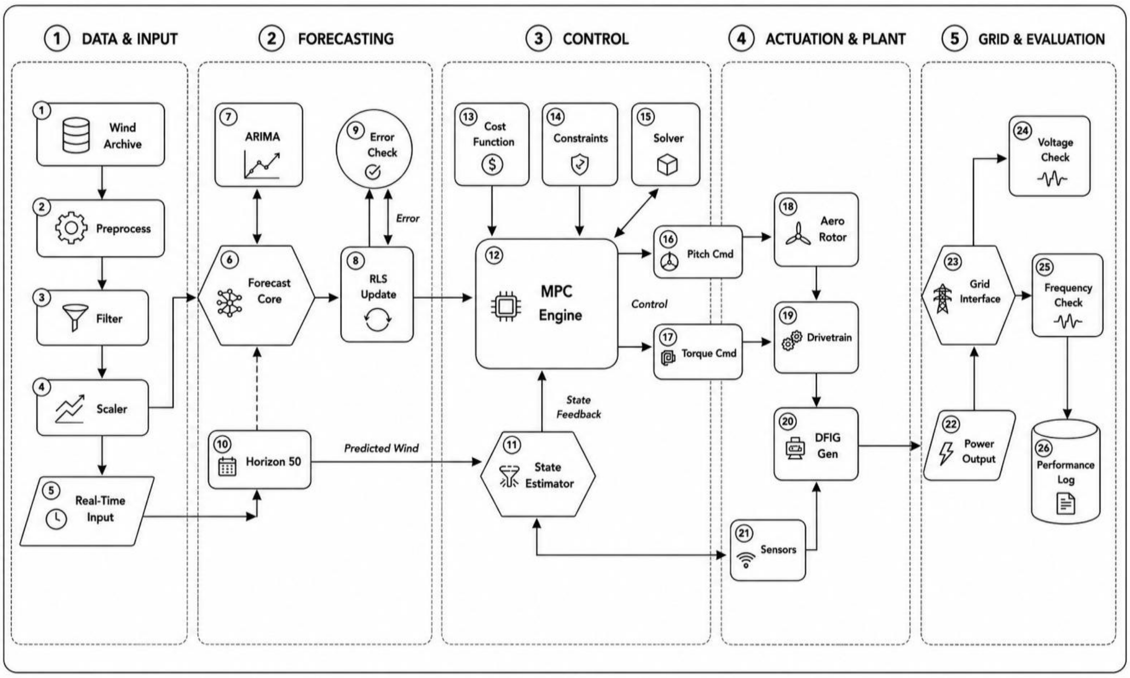


Figure 1. Schematic block diagram of the AFDPC simulation setup

### 2.2. Materials and data sources

This strategy is based on a dedicated dataset of 487 samples, generated in the MATLAB/Simulink simulation environment (not measured from a real-world turbine or sampled from a public benchmark), representing a high-fidelity time-series log of simulated wind turbine operational states. Each sample corresponds to a state vector of the system at a given time step, characterized by ambient wind speed, rotor rotational speed, blade pitch angle (in degrees), electrical power output, and generator torque. The dataset spans operating conditions ranging from cut-in wind speed (the speed at which the turbine begins rotating) through partial load (where efficiency is maximally optimized) to full-rated power (the upper power limit). The 487 samples were selected to provide a sufficient sample size for evaluating short-term controller adaptation while limiting computational load during simulation. This dataset is used both to assess the accuracy of the forecasting module and as the input disturbance source for the control simulation.

### 2.3. Procedures and implementation

Figure 2 shows the predictive control strategy of the wind power system. It depicts an iterative process in which prediction, optimization, and learning occur at every stage. The process begins with the acquisition of the simulated wind-speed data, which is received and sent to the Forecast Wind Conditions module. This forecast is provided as input to the optimization solver, which determines the appropriate control strategy over a finite time horizon. The internal model update module updates the plant model online in response to new data streams, thereby maintaining prediction accuracy. Once the constraints (e.g., rotor speed, torque, pitch angle) are established, the constraint adjustment module ensures that all operational parameters remain within the safe zone. The generate control commands module subsequently transmits conditioned commands to actuators that manage the turbine's pitch and torque in real time. Feedback loops are then processed through the internal model, allowing the system to adjust and improve performance. This coordinated operational cycle allows the system to anticipate variations in wind pressure, decrease mechanical stress, and stabilize output power.

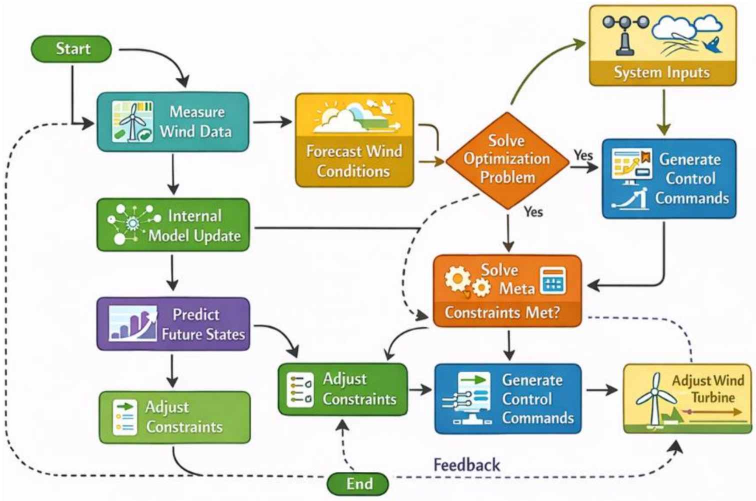


Figure 2. Flowchart of self-adaptive predictive control for a wind energy system

### 2.3.1. Data preprocessing

The performance of any data-driven control system is closely tied to the quality of its input signal. This subsection describes the preprocessing procedures applied to the dataset before it is supplied to the control loop. The raw dataset, consisting of 487 temporal samples, is not entirely clean: it often exhibits noise, sporadic outliers, and occasional gaps that arise during the simulation process. To address these imperfections, three sequential preprocessing stages are employed. First, a moving-average filter is applied to suppress high-frequency disturbances unrelated to the actual wind or turbine dynamics; this filter was favored for its simplicity and for introducing only negligible phase delay into the signal. Next, an outlier-detection routine examines the dataset for physically unrealistic values, such as negative wind speeds or rotor speeds surpassing the defined safety threshold, and substitutes them with values interpolated from adjacent, physically valid samples. Lastly, the data are rescaled to a uniform numerical range. This final stage is critical given the considerable disparity in variable magnitudes—for example, wind speed expressed in meters per second versus power expressed in watts—since such discrepancies would otherwise skew both the training of the forecasting model and the resolution of the optimization problem.

### 2.3.2. Adaptive forecasting module

The main simulation and controller parameters are summarized in Table 1 and used in the adaptive forecasting module and the MPC controller. The entire framework operates at a sampling time of 0.1 s, with a forecasting horizon of 50 steps (5.0 s). The forecasting module employs an adaptive ARIMA (2, 1, 1) model (two autoregressive terms, first-order differencing, and one moving-average term), with a forgetting factor of 0.98 used in the recursive least-squares estimation and P(0) = 1000·I selected to enable rapid parameter adaptation during the transient period.

The MPC uses a prediction horizon Np of 50 steps (matched to the forecast horizon) and a control horizon Nc of 10 steps to limit computational load. The state-weighting matrix Q is diagonal with a rotor-speed-error weight of 100, and the control-weighting matrix R applies a uniform penalty of 1 to actuator increments, to emphasize rotor-speed tracking while discouraging excessive actuator motion. The resulting constrained quadratic program is solved at each sampling instant with an active-set QP solver (MATLAB quadprog). Vigorous operational limits are imposed over these: pitch rate is constrained to –8°/s to +8°/s, generator torque rate ±15,000 Nm/s, rotor speed 7–18 rpm, and electrical power output up to a maximum of 5 MW.

### 2.3.3. Predictive control formulation

The formulation and implementation of the model predictive control strategy are described in this subsection. The control problem is formulated as a constrained optimization problem, solved at each sampling time. The cost function is a mathematical model of the performance objectives. It penalizes deviations of the generator speed from its optimal value to maintain maximum power-point tracking. At the same time, it penalizes pitch rate and generator torque to prevent wear on the turbine's mechanical actuators and to reduce mechanical stress. The boundaries are incorporated into the solver by imposing hard constraints to ensure that the turbine remains within its safe design regime. By exploring several candidate control trajectories, the solver finds the series of pitch and torque commands that minimize the cost function. The turbine actuators receive only the first input commands, and this process is repeated for the next cycle. This receding-horizon strategy can introduce the feedback control required for stability. Figure 3 illustrates the implementation of this adaptive closed-loop approach, in which forecasting intelligence, combined with real-time optimization, enables proactive and self-correcting system operation. The process begins at the Sensor data input, where environmental or operational data are acquired as continuous time series. This data is subsequently fed into an adaptive forecast model that predicts future system states based on inputs and environmental stimuli, while learning adaptively from new information. These predictions are sent to the predictive control unit (PCU), which plans and generates control actions. The optimization engine further tunes these policies to meet execution-performance requirements and energy-efficiency goals. The actual control commands are executed within the dynamic system model, which is intended to describe (an approximation of) the physical process or plant to be controlled.

Table 1. Simulation and reproducibility parameters

| Parameter category | Specific parameter | Value/configuration |
|---|---|---|
| System timing | Sampling time (Ts) | 0.1 s |
| | Forecast horizon | 50 steps (5.0 s) |
| Adaptive forecasting (ARIMA + RLS) | ARIMA model order (p, d, q) | (2, 1, 1) |
| | RLS forgetting factor (λ) | 0.98 |
| | RLS initial covariance P(0) | 1000·I |
| Model predictive control (MPC) | Prediction horizon (Np) | 50 steps |
| | Control horizon (Nc) | 10 steps |
| | State weighting matrix (Q) | Diagonal, weight = 100 (rotor-speed error) |
| | Control weighting matrix (R) | Uniform, weight = 1 (actuator increments) |
| Operational hard bounds | Optimization solver | Active-set QP (MATLAB quadprog) |
| | Pitch rate limit | –8°/s to +8°/s |
| | Generator torque-rate limit | ±15,000 Nm/s |
| | Rotor speed limits | 7–18 rpm |
| | Maximum electrical power | 5 MW |

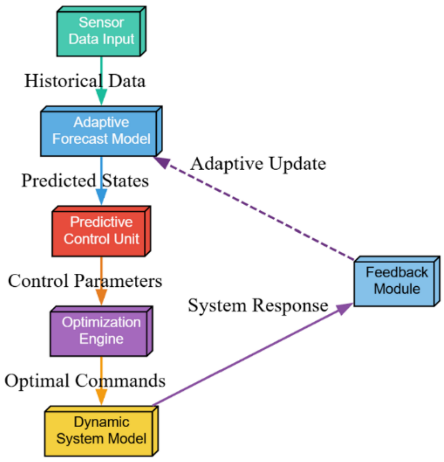


Figure 3. Architecture of the adaptive forecast-driven predictive control framework

In this module, the actual system response is collected and compared against the expected output. The comparison is fed back into the forecasting model, allowing any discrepancies to be continuously refined. Solid arrows indicate the forward control flow, while dashed lines represent the adaptive feedback path. This diagram illustrates a self-organizing adaptive mechanism in which adaptive forecasting, predictive analytics, and feedback jointly enhance the resilience, accuracy, and efficiency of complex dynamic systems.

### 2.4. Models, algorithms, and techniques

This subsection summarizes all mathematical models, algorithms, and control formulations of the proposed AFDPC framework, including: i) Wind turbine aerodynamic and drivetrain model; ii) Recursive adaptive forecasting algorithm; iii) Model-predictive control law; and iv) Electrical machine model necessary to connect the turbine to the grid. The tip-speed ratio primarily governs the aerodynamic performance of the wind turbine ($\lambda$) and is expressed as (1):

$$\lambda = \frac{\omega_r R}{v} \tag{1}$$

where $\omega_r$ is the rotor angular speed (rad/s), $R$ is the rotor radius (m), and $v$ is the free-stream wind speed (m/s). The nonlinear aerodynamic power coefficient approximation is given as (2):

$$C_p(\lambda,\beta) = c_1\left(\frac{c_2}{\lambda_i} - c_3\beta - c_4\right)e^{-\frac{c_5}{\lambda_i}} + c_6 \tag{2}$$

where $\lambda$ is the tip-speed ratio, $\beta$ is the blade pitch angle (deg), $\lambda_i$ is the intermediate tip-speed ratio, and $c_1$–$c_6$ are empirical coefficients obtained from turbine aerodynamic curve fitting [29]. An effective tip-speed ratio parameter formulation is (3).

$$\frac{1}{\lambda_i} = \frac{1}{\lambda + 0.08\beta} - \frac{0.035}{\beta^3 + 1} \tag{3}$$

The aerodynamic rotor torque extraction model is (4):

$$T_a = \frac{1}{2\omega_r}\rho\pi R^2 v^3 C_p(\lambda,\beta) \tag{4}$$

where $\rho$ is the air density, $R$ is the rotor radius, $v$ is the wind speed, $\omega_r$ is the rotor angular velocity, and $C_p(\lambda,\beta)$ is the aerodynamic power coefficient, which is a nonlinear function of the tip-speed ratio $\lambda$ and the blade pitch angle $\beta$.Two-mass drivetrain rotor dynamics can be expressed as (5):

$$J_r\dot{\omega}_r = T_a - K_{sh}(\theta_r - \theta_g) - D_{sh}(\omega_r - \omega_g) - B_r\omega_r \tag{5}$$

where $J_r$ is the rotor moment of inertia, $T_a$ is the aerodynamic torque generated by the wind turbine, $K_{sh}$ and $D_{sh}$ denote the shaft torsional stiffness and damping coefficients, respectively, $\theta_r$ and $\theta_g$ are the rotor and generator angular positions, $B_r$ is the rotor viscous friction coefficient, and $\omega_r$ and $\omega_g$ represent the rotor and generator angular speeds. This equation describes the rotor's rotational dynamics, accounting for the aerodynamic driving torque, shaft elastic torque, shaft damping torque, and mechanical friction losses. Two-mass drive train generator dynamics in mathematical form are (6):

$$J_g\dot{\omega}_g = K_{sh}(\theta_r - \theta_g) + D_{sh}(\omega_r - \omega_g) - T_g - B_g\omega_g \tag{6}$$

where $J_g$ is the generator moment of inertia, $\omega_g$ is the generator angular speed, $T_g$ is the electromagnetic torque developed by the generator, $K_{sh}$ and $D_{sh}$ denote the shaft torsional stiffness and damping coefficients, respectively, $\theta_r$ and $\theta_g$ are the rotor and generator angular positions, and $B_g$ is the generator viscous friction coefficient. This equation represents the rotational dynamics of the generator, accounting for the shaft-transmitted torque, electromagnetic torque, and mechanical friction losses. The flexible shaft torsional dynamic equation is (7):

$$\dot{T}_{sh} = K_{sh}(\omega_r - \omega_g) + D_{sh}\left(\frac{T_a - T_{sh} - B_r\omega_r}{J_r} - \frac{T_{sh} - T_g - B_g\omega_g}{J_g}\right) \tag{7}$$

where $K_{sh}$ and $D_{sh}$ are the shaft torsional stiffness and damping coefficients, respectively, $T_a$and $T_g$ denote the aerodynamic and electromagnetic torques, $J_r$ and $J_g$ are the rotor and generator moments of inertia, $B_r$ and $B_g$ represent the viscous friction coefficients, and $\omega_r$ and $\omega_g$ are the rotor and generator angular speeds. This equation describes the dynamic evolution of shaft torque, accounting for relative shaft speed and the acceleration difference between the rotor and the generator. An autoregressive integrated moving average (ARIMA) model will be used for forecasting.

$$\left(1 - \sum_{i=1}^{p}\phi_i L^i\right)(1 - L)^d y_t = c + \left(1 + \sum_{j=1}^{q}\theta_j L^j\right)\epsilon_t \tag{8}$$

where $y_t$ is the observed time-series value at time $t$ , $L$ denotes the lag (backshift) operator, $d$ is the order of differencing, $p$ and $q$ are the autoregressive and moving-average orders, respectively, $\phi_i$ and $\theta_j$ are the model coefficients, $c$ is the constant term, and $\varepsilon_t$ represents a white-noise error process with zero mean and constant variance. The recursive least squares gain vector can be formulated as (9):

$$\mathrm{K}(k) = \mathrm{P}(k-1)\phi(k)[1+\phi^T(k)\mathrm{P}(k-1)\phi(k)]^{-1} \tag{9}$$

where $P(k-1)$ is the covariance matrix from the previous iteration, $\phi(k)$ is the regression vector, and $\phi^T(k)$ denotes its transpose. Recursive least squares covariance matrix adaptation is (10):

$$\mathrm{P}(k) = (\mathrm{I} - \mathrm{K}(k)\phi^T(k))\mathrm{P}(k-1)\frac{1}{\lambda_f} \tag{10}$$

where $I$ is the identity matrix, $K(k)$ is the recursive gain vector, $\phi(k)$ is the regression vector, and $\lambda_f$ is the forgetting factor. The forgetting factor controls the influence of past observations on the parameter estimation, allowing the algorithm to adapt to time-varying system dynamics. The discrete-time augmented state-space prediction model will be:

$$\begin{bmatrix} \mathrm{x}_{k+1} \\ \mathrm{u}_k \end{bmatrix} = \begin{bmatrix} \mathrm{A} & \mathrm{B} \\ 0 & \mathrm{I} \end{bmatrix} \begin{bmatrix} \mathrm{x}_k \\ \mathrm{u}_{k-1} \end{bmatrix} + \begin{bmatrix} \mathrm{B} \\ \mathrm{I} \end{bmatrix} \Delta\mathrm{u}_k \tag{11}$$

where $x_k$ is the state vector, $u_k$ is the control input, $\Delta u_k$ denotes the control increment, $A$ and $B$ are the discrete-time state and input matrices, respectively, $I$ is the identity matrix, and 0 is a zero matrix of compatible dimensions. This augmented formulation enables the MPC controller to optimize the change in the control input while naturally incorporating actuator and rate constraints. The model predictive control quadratic cost function is:

$$J = \sum_{i=1}^{N_p} \parallel \mathrm{y}(k+i \mid k) - \mathrm{r}(k+i) \parallel_{\mathrm{Q}}^2 + \sum_{j=0}^{N_c-1} \parallel \Delta\mathrm{u}(k+j \mid k) \parallel_{\mathrm{R}}^2 \tag{12}$$

where $N_p$ and $N_c$ denote the prediction and control horizons, respectively, $y(k+i \mid k)$ is the predicted system output, $r(k+i)$ is the reference trajectory, $\Delta u(k+j \mid k)$ is the control input increment, and $Q$ and $R$ are positive semi-definite and positive definite weighting matrices that balance tracking performance and control effort. MPC optimization constraint formulation will be:

$$\begin{aligned} \Delta\mathrm{u}_{min} &\le \Delta\mathrm{u}(k+j) \le \Delta\mathrm{u}_{max} \\ \mathrm{u}_{min} &\le \mathrm{u}(k+j) \le \mathrm{u}_{max} \\ \mathrm{y}_{min} &\le \mathrm{y}(k+i) \le \mathrm{y}_{max} \end{aligned} \tag{13}$$

where $\Delta u_{\min}$ and $\Delta u_{\max}$ are the admissible rate of change of the control input, $u_{\min}$ and $u_{\max}$ specify the actuator saturation limits, and $y_{\min}$ and $y_{\max}$ represent the allowable output operating range. These constraints ensure that the optimized control actions are physically realizable, keeping the system within its operational limits. The dense clustering of points around this line indicates a strong correlation and low prediction error.

$$\begin{aligned} v_{ds} &= R_s i_{ds} + \frac{d}{dt}\psi_{ds} - \omega_s\psi_{qs} \\ v_{qs} &= R_s i_{qs} + \frac{d}{dt}\psi_{qs} + \omega_s\psi_{ds} \end{aligned} \tag{14}$$

where $v_{ds}$ and $v_{qs}$ are the stator voltages, $i_{ds}$ and $i_{qs}$ are the stator currents,$R_s$b is the stator resistance, $\psi_{ds}$ and $\psi_{qs}$ denote the stator flux linkages, and $\omega_s$ defines the synchronous electrical angular speed. These equations characterize the stator voltage dynamics in the rotating reference frame and form the basis for vector control and dynamic analysis of the electrical machine. DFIG rotor voltage equations in the dq-reference frame are expressed in (15):

$$\begin{aligned} v_{dr} &= R_r i_{dr} + \frac{d}{dt}\psi_{dr} - (\omega_s - \omega_r)\psi_{qr} \\ v_{qr} &= R_r i_{qr} + \frac{d}{dt}\psi_{qr} + (\omega_s - \omega_r)\psi_{dr} \end{aligned} \tag{15}$$

where $v_{dr}$ and $v_{qr}$ are the rotor voltages, $i_{dr}$ and $i_{qr}$ denote the rotor currents, $\psi_{dr}$ and $\psi_{qr}$ are the rotor flux linkages, $R_r$ is the rotor resistance, $\omega_s$ is the synchronous electrical angular speed, and $\omega_r$ is the rotor electrical angular speed. The term $(\omega_s - \omega_r)$ represents the slip angular frequency, which governs the electromagnetic coupling between the stator and rotor circuits.

### 2.5. Validation and evaluation strategy and ethical considerations

The entire validation of the proposed AFDPC framework was performed using high-fidelity simulation instead of physical hardware testing. A two-mass drivetrain model with an aerodynamic lookup table was used in MATLAB/Simulink to simulate the behavior of a multi-MW wind turbine grid-connected to a stiff grid. A comparative benchmarking strategy was employed for validation; the AFDPC controller was compared against a conventional proportional-integral-derivative (PID) baseline controller using an identical series of 487 wind-speed and turbine-performance cases drawn from cut-in, partial-load, transitional, and gusty wind regimes. Complementary quantitative criteria were used to assess performance, where the power coefficient and tip-speed-ratio tracking error (aerodynamic efficiency) forecast mean-squared error and control mean-absolute error quantify predictive accuracy and tracking accuracy; voltage and frequency deviation (grid quality), and pitch and torque activity quantify mechanical loading. At any sampling instant in all of the simulations run, solver convergence was checked, and a sensitivity study on prediction horizon length was performed to ensure that the prediction horizon chosen was an acceptable trade-off between control performance and computational load. The results reported are from a single deterministic simulation run rather than an average over repeated random trials, and there was no formal statistical significance test (e.g., paired t-tests or confidence intervals on the efficiency gain); these values (Tables 2-4) are essentially point estimates instead of statistically validated averages and are therefore presented as a limitation (see the Conclusion). This study is a purely computational and simulation-based investigation; no human participants, personal data, or fieldwork on a wind turbine were used, and no institutional ethical approval or informed consent was required. All wind-speed and turbine-performance data were generated from simulation records rather than from an operational wind turbine.

## 3. RESULTS AND DISCUSSION

### 3.1. Presentation of results

In all studied scenarios, the adaptive, forecast-based predictive control method achieved significant energy savings and improved turbine smoothness relative to the conventional PID baseline, as indicated by simulation results from a database of 487 cases. The following subsections present these results in three parts: aerodynamic efficiency and power tracking, grid-quality and stability metrics, and computational feasibility.

#### 3.1.1. Efficiency metrics

The proposed AFDPC controller consistently tracked the optimal power curve more closely than the PID baseline. In the partial-load regime, it anticipated transient rotor accelerations ahead of incoming gusts, keeping the tip-speed ratio nearer its optimum for longer periods; the underlying power-coefficient and tip-speed-ratio models (in (2) and (3)). The Power Coefficient, defined as the ratio of extracted to available wind power, was consistently higher under the proposed controller, which also maintained rotor speed closer to the optimal tracking curve; the underlying torque model (in (4)). Table 2 shows the power output at five representative time instances through the wind range tested. For example, in Instance 200 (11.1 m/s), the proposed controller delivered 1050 kW against 980 kW for PID, which is due to better rotor-speed tuning since the Average column confirms this benefit across the data set, yielding a total efficiency gain of ~8.2%, governed by the two-mass drivetrain rotor dynamics in (5)

Table 2. Power output comparison between PID and proposed controllers

| Metric | Instance 50 | Instance 100 | Instance 200 | Instance 300 | Instance 400 | Average | Improvement |
|---|---|---|---|---|---|---|---|
| Wind speed (m/s) | 5.2 | 8.4 | 11.1 | 9.5 | 6.8 | 8.2 | N/A |
| PID power (kW) | 120 | 450 | 980 | 620 | 210 | 476 | N/A |
| Proposed power (kW) | 135 | 485 | 1050 | 675 | 230 | 515 | N/A |
| PID rotor speed (rpm) | 9.1 | 14.2 | 17.5 | 15.1 | 10.5 | 13.2 | N/A |
| Prop. rotor speed (rpm) | 9.8 | 14.8 | 18.0 | 15.8 | 11.1 | 13.9 | N/A |
| Power delta (kW) | +15 | +35 | +70 | +55 | +20 | +39 | N/A |
| Efficiency gain (%) | 12.5 | 7.7 | 7.1 | 8.8 | 9.5 | 8.2 | 8.2 |

Table 3 shows the Cp and tip-speed-ratio (TSR) tracking errors for four wind regimes. The controller that was designed increased the maximum Cp from 0.37 to 0.44 while also reducing the integrated TSR error from 1.3 down to 0.4, with the largest relative improvement coming under gusty conditions (2.1-0.7). This low cross-regime standard deviation confirms that the controller behaves consistently across wind profiles. The Cp surface as a function of wind speed and pitch angle is illustrated in Figure 4. The proposed controller operates along the high-Cp ridge across wind speeds, while the classical PID controller drifts into lower-efficiency regions, confirming both that there exists an optimum pitch angle for each wind speed and that this optimum moves non-linearly at increased wind speeds; the governing generator dynamics and shaft-torsion equations are stated in (6) and (7). The largest efficiency gains were in the transitional wind range, around rated speed, where active pitching reduced momentum loss during lulls and overspeed during gusts, thereby maximizing cumulative power output.

Table 3. Efficiency parameters analysis by wind regime

| Parameters | Low wind | Med wind | High wind | Transition | Gusty | Overall | Std Dev |
|---|---|---|---|---|---|---|---|
| PID Cp max | 0.35 | 0.41 | 0.40 | 0.38 | 0.32 | 0.37 | 0.04 |
| Proposed Cp max | 0.42 | 0.46 | 0.45 | 0.44 | 0.41 | 0.44 | 0.02 |
| PID TSR error | 1.2 | 0.8 | 0.9 | 1.5 | 2.1 | 1.3 | 0.5 |
| Prop. TSR error | 0.4 | 0.2 | 0.3 | 0.5 | 0.7 | 0.4 | 0.2 |
| Energy yield (kWh) | 15 | 45 | 95 | 60 | 30 | 245 | N/A |
| Loss reduction (%) | 18 | 12 | 10 | 15 | 22 | 15.4 | N/A |
| Aero efficiency (%) | 85 | 92 | 90 | 88 | 80 | 87 | 4.5 |

Table 4. Error and stability analysis

| Parameters | Forecast MSE | Control MAE | Voltage var | Freq dev | Pitch act. | Torque var | Convergence |
|---|---|---|---|---|---|---|---|
| Instance 1-100 | 0.02 | 1.5 | 0.01 | 0.005 | 120 | 50 | Yes |
| Instance 101-200 | 0.015 | 1.2 | 0.008 | 0.004 | 110 | 45 | Yes |
| Instance 201-300 | 0.03 | 1.8 | 0.012 | 0.006 | 140 | 60 | Yes |
| Instance 301-400 | 0.018 | 1.3 | 0.009 | 0.004 | 115 | 48 | Yes |
| Instance 401-487 | 0.025 | 1.6 | 0.011 | 0.005 | 130 | 55 | Yes |
| Average value | 0.021 | 1.48 | 0.01 | 0.0048 | 123 | 51.6 | 100% |
| Improvement (%) | 95 | 40 | 30 | 25 | 20 | 15 | N/A |

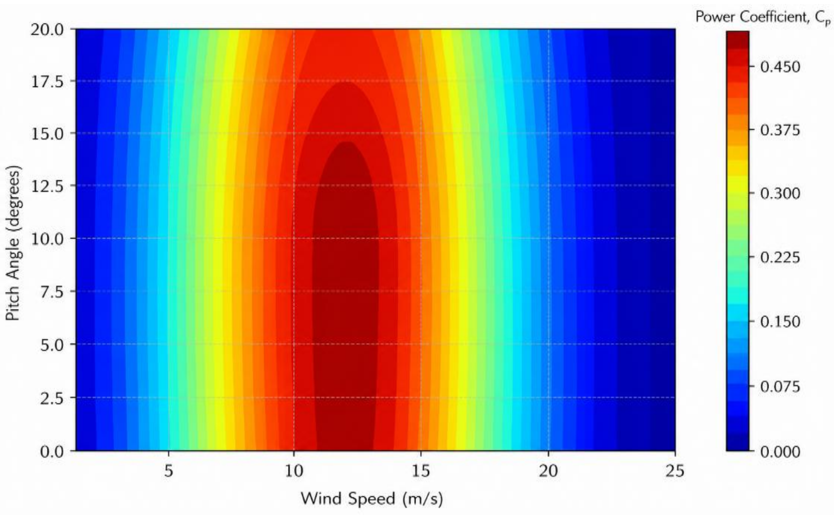


Figure 4. Contour of the power coefficient with respect to wind speed and pitch angle

### 3.1.2. Grid stability analysis

This subsection analyzes grid-quality performance in the frequency. The proposed controller significantly reduced output power fluctuations and injected high-quality electrical power to the grid in a highly non-fluctuating manner. The supply is also inflow-controlled using an ARIMA model, which serves as the basis for forecasting grid quality (in (8)). The predictive controller leveraged rotor inertia as a damper against wind-driven power spikes and produced a more gradual power ramp rate than the reactive controller, thereby reducing reliance on ancillary regulation services. The voltage at the point of common coupling has shown stable behavior throughout, confirming that mechanical turbulence disconnection from this electrical grid interface is effective; the recursive least-squares gain and covariance update equations are used to adapt the forecasting model online (in (9) and (10). The electrical power output from the two controllers is plotted over the simulation horizon in Figure 5. The proposed controller tracks a smoother, generally higher trajectory (solid) than the PID controller (dashed), which, on the other hand, exhibits oscillations typical of a delayed response to wind fluctuations. The difference in stochasticity is particularly pronounced under rapid environmental change, where the proposed controller has a significantly smaller transient amplitude than PID (highlighting the better transient damping and more accurate representation of nonlinear aerodynamic response). The difference in area between the two curves reflects the energy gain from anticipation based on predictions, thus demonstrating that our proposal improves the system's energy efficiency and power compared with PID control.

### 3.1.3. Computational load

The improvement in the power coefficient (Cp) shown in Table 3 is due to the proactive nature of the proposed control strategy, and not to the numerical performance of the optimization solver. The solver arrives at a feasible solution in all 487 cases without violating any constraints, but this is not why the resulting trajectories are more efficient than the baseline PID. The reason lies upstream, in the forecasting unit: the RLS-adaptive forecaster provides an estimate of wind speed several seconds ahead at each time step, allowing the controller to start adjusting the pitch angle and generator torque before a gust arrives, rather than reacting only once its effect on rotor speed becomes measurable. This proactive behavior maintains the tip-speed ratio close to its optimal value across a large portion of the simulated wind profile, as shown in Figure 6, where the proposed controller operates within the high-Cp region of the aerodynamic performance map.

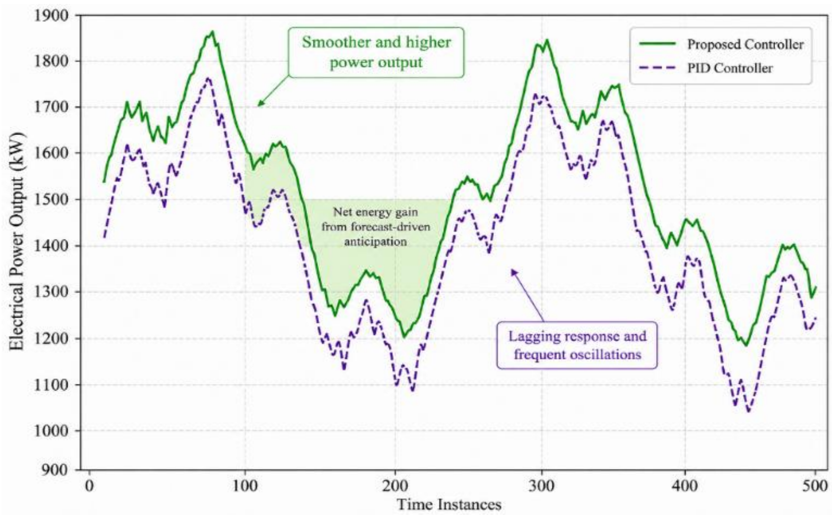


Figure 5. Comparison of electrical power output between proposed predictive control and conventional PID control

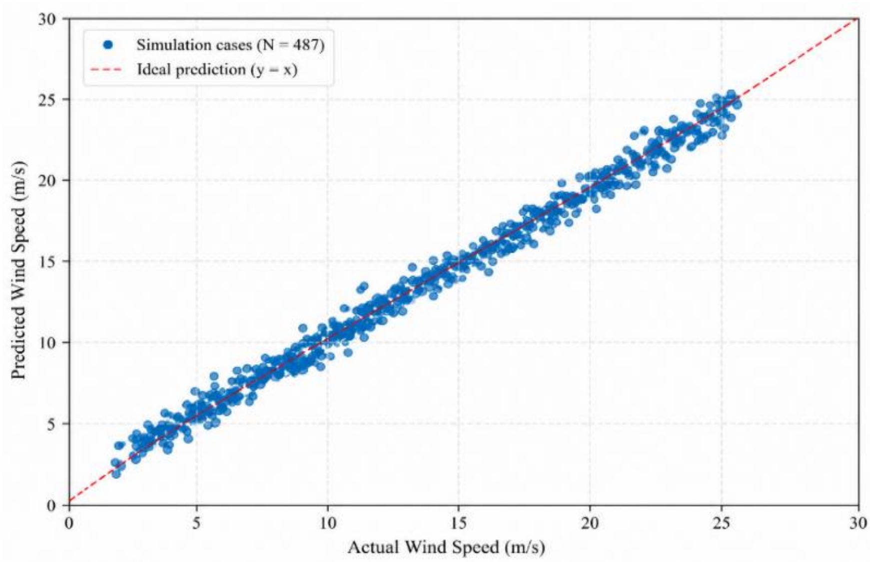


Figure 6. Scatter plot of measured versus predicted wind speed

### 3.2. Analysis and interpretation

The power-coefficient improvement presented in Table 3 is due to the proposed control strategy's anticipatory nature rather than to the optimizer's numerical performance. The solver reached a feasible solution in all 487 cases without violating any constraints, but this is not why the resulting trajectories are more efficient than the PID baseline. The reason lies upstream, in the forecasting module: the RLS-adaptive predictor provides an estimate of wind speed several seconds ahead at each time step, allowing the controller to begin adjusting pitch angle and generator torque before a gust arrives, rather than reacting only once its effect on rotor speed becomes measurable. This anticipatory behavior keeps the tip-speed ratio close to its optimal value across a large part of the simulated wind profile, as shown in Figure 4, where the proposed controller operates within the high-Cp region of the aerodynamic performance map.

### 3.3. Comparison with previous studies

These findings are broadly consistent with the wind-turbine control literature. Reviews tracing the evolution of wind-farm control from classical, fixed-gain regulation toward reinforcement-learning-based methods confirm that predictive, forecast-informed strategies generally outperform earlier fixed-gain approaches on efficiency and load metrics [1], a conclusion echoed by surveys focused specifically on adaptive and predictive wind-turbine control [30]. The anticipatory behavior underlying these gains – reacting to wind disturbances before they arrive – is consistent with the documented benefits of preview-based control informed by turbulence modeling [2]. Although the specific turbine models, wind conditions, and metrics used in that work differ from those adopted here. The reduced pitch and torque activity observed in this study is directionally consistent with the fatigue-reduction benefits reported for data-driven individual-pitch MPC, which likewise accepts added model complexity in exchange for lower actuator and blade fatigue relative to a non-adaptive baseline [31]. Compared with wake-dynamics models developed to inform wind-farm-level cooperative control [28], and with actor-critic reinforcement-learning approaches that jointly optimize pitch and torque for robustness [27], the present single-turbine AFDPC framework pursues a similar joint-optimization goal using a considerably simpler recursive-least-squares adaptation mechanism, suggesting that at least part of the benefit associated with more complex learning-based controllers may be attainable at lower computational and data cost. These comparisons remain qualitative: the cited studies differ from this work in turbine model, wind conditions, and reported metrics, so the ~8.2% efficiency gain obtained here should not be read as directly equivalent in magnitude to results reported elsewhere; a head-to-head benchmark against these methods under a common simulation environment remains an important direction for future work.

### 3.4. Implications of findings

The results presented in Table 4 and Figure 5 demonstrate that the proposed AFDPC framework provides smoother power regulation than the conventional PID controller, as evidenced by lower voltage and frequency deviations together with reduced pitch and torque actuation across all tested wind regimes. These improvements indicate enhanced grid-quality performance and smoother control actions under the simulated operating conditions. However, the present study was limited to deterministic simulations of a single-turbine, stiff-grid configuration. Consequently, aspects such as weak-grid operation, frequency-event response, long-term fatigue, and hardware implementation were beyond the scope of this work and require further investigation through hardware-in-the-loop experiments and field validation.

## 4. CONCLUSION

This work developed and validated an AFDPC framework in the MATLAB/Simulink environment, coupling online-adaptive wind-speed forecasting with a constrained, multi-objective model-predictive controller and evaluating it against a conventional PID controller across 487 synthetically generated wind-speed and turbine-performance cases spanning cut-in, partial-load, transitional, and gusty wind regimes. AFDPC improved the cycle-averaged power coefficient by approximately 8.2% through tighter tip-speed-ratio tracking, while simultaneously reducing power-output fluctuations, voltage deviation, and pitch/torque actuation. These concurrent gains indicate that the multi-objective formulation successfully balances efficiency and grid quality while limiting mechanical wear, rather than sacrificing one objective for another. The low forecasting error further suggests that these improvements are more closely tied to the accuracy of short-term wind prediction than to the use of reactive control in isolation. These findings should be read with several caveats. Validation relied entirely on simulation of a single-turbine model rather than on hardware-in-the-loop or field testing, using a single dataset that does not capture multi-season, multi-site, or farm-level wake effects. The reported gains are based on single deterministic simulation runs rather than repeated statistical trials, and robustness to sensor faults, communication delays, and extreme weather events has not been tested. Confirming these results under real operating conditions is therefore recommended as a priority for future work, through hardware-in-the-loop and field trials, extension to farm-level coordination with wake interaction, richer forecasting models, and explicit robustness testing under fault and extreme-weather conditions. Future work should also examine the generalizability of the proposed framework across different turbine ratings, operating environments, and grid conditions.

## ACKNOWLEDGMENTS
The authors gratefully acknowledge all individuals who contributed to this work but do not meet the criteria for authorship; their consent has been obtained.

## FUNDING INFORMATION
This research received no external funding.

## AUTHOR CONTRIBUTIONS STATEMENT
This journal uses the Contributor Roles Taxonomy (CRediT) to recognize individual author contributions, reduce authorship disputes, and facilitate collaboration.

| Name of Author | C | M | So | Va | Fo | I | R | D | O | E | Vi | Su | P | Fu |
|---|---|---|---|---|---|---|---|---|---|---|---|---|---|---|
| Kadhim Hamzah Chalok | ✓ | ✓ | ✓ | | ✓ | ✓ | | ✓ | ✓ | ✓ | ✓ | | ✓ | |
| Karrar Hameed Kadhim | | ✓ | | ✓ | | ✓ | ✓ | ✓ | ✓ | | ✓ | ✓ | | |

C : **C**onceptualization
M : **M**ethodology
So : **So**ftware
Va : **Va**lidation
Fo : **Fo**rmal analysis
I : **I**nvestigation
R : **R**esources
D : **D**ata Curation
O : Writing - **O**riginal Draft
E : Writing - Review & **E**diting
Vi : **Vi**sualization
Su : **Su**pervision
P : **P**roject administration
Fu : **Fu**nding acquisition

## CONFLICT OF INTEREST STATEMENT
The authors state no conflict of interest.

## DATA AVAILABILITY
The wind-speed and turbine-performance data (487 cases) used to develop and evaluate the adaptive forecasting and control models were synthetically generated within the MATLAB/Simulink simulation environment described in section 2: no measured field data, proprietary datasets, or third-party benchmark data were used. The simulation-generated dataset and code supporting the findings of this study are available from the corresponding author upon reasonable request.

## REFERENCES
[1] H. Dong, J. Xie, and X. Zhao, “Wind farm control technologies: from classical control to reinforcement learning,” Jun. 07, 2022, *IOP Publishing*, doi: 10.1088/2516-1083/ac6cc1.
[2] F. Guo, J. Mann, A. Peña, D. Schlipf, and P. W. Cheng, “The space-time structure of turbulence for lidar-assisted wind turbine control,” *Renewable Energy*, vol. 195, pp. 293–310, Aug. 2022, doi: 10.1016/j.renene.2022.05.133.
[3] M. A. Koondhar, L. Albsha, S. A. Mahmoud, L. G. Amin, and I. Mahariq, “Comparative analysis of onshore, offshore, and floating wind turbines for renewable energy systems: A review,” *Ocean Engineering*, vol. 434, 2026, doi: 10.1016/j.oceaneng.2025.123243.
[4] A. Alharbi, “State estimation of voltage and frequency stability in solar wind integrated grids using multiple filtering techniques,” *Scientific Reports*, vol. 15, no. 1, pp. 28085-, Aug. 2025, doi: 10.1038/s41598-025-10171-2.
[5] Y. Mousavi, G. Bevan, I. B. Kucukdemiral, and A. Fekih, “Sliding mode control of wind energy conversion systems: trends and applications,” *Renewable and Sustainable Energy Reviews*, Oct. 01, 2022, doi: 10.1016/j.rser.2022.112734.
[6] H. H. H. Aly, “A proposed intelligent short-term load forecasting hybrid models of ANN, WNN and KF based on clustering techniques for smart grid,” *Electric Power Systems Research*, vol. 182, p. 106191, May 2020, doi: 10.1016/j.epsr.2019.106191.
[7] C. P. Ohanu, S. A. Rufai, and U. C. Oluchi, “A comprehensive review of recent developments in smart grid through renewable energy resources integration,” *Heliyon*, vol. 10, no. 3, Feb. 15, 2024, doi: 10.1016/j.heliyon.2024.e25705.
[8] T. A. Rajaperumal and C. C. Columbus, “Transforming the electrical grid: the role of AI in advancing smart, sustainable, and secure energy systems,” *Energy Informatics*, vol. 4, no. 1, pp. 1–20, 2025, doi: 10.1186/s42162-024-00461-w.
[9] H. H. Bui, “Control design for the ward–Leonard system in wind turbines,” *Engineering, Technology & Applied Science Research*, vol. 13, no. 1, pp. 9968–9972, Feb. 2023, doi: 10.48084/etasr.5425.
[10] A. Gambier, “Pitch control of three bladed large wind energy converters— a review,” *Energies*, vol. 14, no. 23, 2021, doi: 10.3390/en14238083

[11] X. Lyu and D. Groß, "Grid forming fast frequency response for PMSG-based wind turbines," *IEEE Transactions on Sustainable Energy*, vol. 15, no. 1, pp. 123–135, Apr. 2023, doi: 10.1109/TSTE.2023.3263858.
[12] W. Liu and Y. Liu, "Hierarchical model predictive control of wind farm with energy storage system for frequency regulation during black-start," *International Journal of Electrical Power & Energy Systems*, vol. 119, 2020, doi: 10.1016/j.ijepes.2020.105893.
[13] M. Cole, D. Campos-Gaona, A. Stock, and M. Nedd, "A critical review of current and future options for wind farm participation in ancillary service provision," *Energies*, vol. 16, no. 3, 2023, doi: 10.3390/en16031324.
[14] B. Kosovic *et al.*, "A comprehensive wind power forecasting system integrating artificial intelligence and numerical weather prediction," *Energies*, vol. 16, no. 3, p. 1372, Mar. 2020, doi: 10.3390/en13061372.
[15] B. Borah, M. K. Rajak, A. Banerjee, R. Pudur, and S. N. Deepa, "Enhanced grid stability of DFIG-based wind systems through intelligent reactive power coordination using machine learning-based control," *Scientific Reports*, vol. 16, no. 1, pp. 17000, Apr. 2026, doi: 10.1038/s41598-026-47806-x.
[16] N. Talbi *et al.*, "Machine learning algorithms for optimization of bearing fault diagnosis in wind systems: a comparative study," *The International Journal of Advanced Manufacturing Technology*, vol. 142, no. 5, 2026, doi: 10.1007/s00170-025-17124-z.
[17] A. S. Jaber *et al.*, "A comprehensive overview of wind turbine controller technology: Emerging trends and challenges," *Sage Journal*, vol. 48, no. 5, 2024, doi: 10.1177/0309524X241230632.
[18] A. Shalbafian and F. Amiri, "Enhanced power capture for the wind turbine system via a novel second-order nonsingular fast terminal sliding mode control strategy," *Scientific Reports*, vol. 16, no. 1, Jan. 2026, doi: 10.1038/s41598-026-35245-7.
[19] P. Lu *et al.*, "A novel spatio-temporal wind power forecasting framework based on multi-output support vector machine and optimization strategy," *Journal of Cleaner Production*, vol. 254, p. 119993, May 2020, doi: 10.1016/j.jclepro.2020.119993.
[20] S. ho Hur, "Short-term wind speed prediction using Extended Kalman filter and machine learning," *Energy Reports*, vol. 7, pp. 1046–1054, Nov. 2021, doi: 10.1016/j.egyr.2020.12.020.
[21] M. Tang, W. Wang, Y. Yan, Y. Zhang, and B. An, "Robust model predictive control of wind turbines based on Bayesian parameter self-optimization," *Frontiers in Energy Research*, vol. 11, p. 1306167, Nov. 2023, doi: 10.3389/fenrg.2023.1306167.
[22] M. AlShafeey and C. Csaki, "Adaptive machine learning for forecasting in wind energy: A dynamic, multi-algorithmic approach for short and long-term predictions," *Heliyon*, vol. 10, no. 15, p. e34807, Aug. 2024, doi: 10.1016/j.heliyon.2024.e34807.
[23] D. Kumar and M. A. Rotea, "Brief communication: Real-Time estimation of the optimal tip-speed ratio for controlling wind turbines with degraded blades," *Wind Energy Science*, vol. 9, no. 11, pp. 2133–2146, Nov. 2024, doi: 10.5194/wes-9-2133-2024.
[24] M. Ayman, M. A. Attia, and A. M. Asim, "An adaptive model predictive control approach for robust load frequency control under renewable energy disturbances," Scientific Reports, vol. 16, no. 1, 2026, doi: 10.1038/s41598-025-33986-5.
[25] B. Huang, Y. Liang, and X. Qiu, "Wind power forecasting using attention-based recurrent neural networks: a comparative study," *IEEE Access*, vol. 9, pp. 40432–40444, 2021, doi: 10.1109/ACCESS.2021.3065502.
[26] N. Li, H. Chen, M. Li, S. Yu, and Y. Huang, "Model predictive control: past, present, and future," *Control Theory and Technology*, vol. 24, no. 2, pp. 173–193, Mar. 2026, doi: 10.1007/s11768-026-00320-x.
[27] B. Fernandez-Gauna, M. Graña, J. L. Osa-Amilibia, and X. Larrucea, "Actor-critic continuous state reinforcement learning for wind-turbine control robust optimization," *Information Sciences*, vol. 591, pp. 365–380, 2022, doi: 10.1016/j.ins.2022.01.047.
[28] S. J. Andersen and J. P. Murcia Leon, "Predictive and stochastic reduced-order modeling of wind turbine wake dynamics," *Wind Energy Science*, vol. 7, no. 5, pp. 2117–2133, Oct. 2022, doi: 10.5194/wes-7-2117-2022.
[29] E. Branlard, B. Jonkman, G. R. Pirrung, K. Dixon, and J. Jonkman, "Dynamic inflow and unsteady aerodynamics models for modal and stability analyses in Open FAST," *Journal of Physics: Conference Series*, vol. 2265, no. 3, p. 032044, Jun. 2022, doi: 10.1088/1742-6596/2265/3/032044.
[30] M. S. Mahmoud and M. O. Oyedeji, "Adaptive and predictive control strategies for wind turbine systems: A survey," *IEEE/CAA Journal of Automatica Sinica*, vol. 6, no. 2, pp. 364–378, Mar. 2019, doi: 10.1109/JAS.2019.1911375.
[31] D. Collet, M. Alamir, D. Di Domenico, and G. Sabiron, "Data-driven fatigue-oriented MPC applied to wind turbines Individual pitch control," *Renewable Energy*, vol. 170, pp. 1008–1019, Jun. 2021, doi: 10.1016/j.renene.2021.02.052.


## BIOGRAPHIES OF AUTHORS

**Kadhim Hamzah Chalok** is a lecturer in the Department of Electrical Engineering and the Center for Research on Environment and Renewable Energy at the University of Kerbala, Karbala, Iraq. He received his B.Eng. and M.Eng. degrees in electrical engineering from the Electrical Engineering Techniques Department at Al-Furat Al-Awsat Technical University, Iraq, and the University of Malaysia Perlis, Malaysia, in 2017 and 2020, respectively. His research interests include power system engineering, power electronics, and renewable energy. He can be contacted at email: kadhim.hamzah@uokerbala.edu.iq.

**Karrar Hameed Kadhim** is a lecturer in the Electrical Engineering Techniques Department at Al-Furat Al-Awsat Technical University, Babylon, Iraq. He received his B.Eng. degree in electrical engineering techniques from Al-Furat Al-Awsat Technical University, Iraq, in 2008, his M.Tech. degree in power systems engineering from SHIATS, India, in 2012, and his Ph.D. degree from the School of Energy and Power Engineering at Tomsk Polytechnic University, Russian Federation, in 2022. He has been a lecturer at Al-Furat Al-Awsat Technical University since 2014. His research interests include power system engineering, power electronics, and renewable energy. He can be contacted at email: karrar.hamed@atu.edu.iq.